Biogeosciences Discuss., 10, 9179–9211, 2013
www.biogeosciences-discuss.net/10/9179/2013/
doi:10.5194/bgd-10-9179-2013

Biogeosciences Discussions
Open Access

On the role of mesoscale eddies for the biological productivity and biogeochemistry in the eastern tropical Pacific Ocean off Peru

L. Stramma[1], H. W. Bange[1], R. Czeschel[1], A. Lorenzo[2], and M. Frank[3]

[1]Helmholtz Centre for Ocean Research Kiel (GEOMAR), Düsternbrooker Weg 20, 24105 Kiel, Germany
[2]Instituto del Mar del Peru (IMARPE), Coastal Laboratory of Pisco, Paracas-Pisco, Peru
[3]Helmholtz Centre for Ocean Research Kiel (GEOMAR), Wischhofstraße 1–3, 24148 Kiel, Germany

Received: 22 May 2013 – Accepted: 23 May 2013 – Published: 10 June 2013

Correspondence to: L. Stramma (lstramma@geomar.de)

Published by Copernicus Publications on behalf of the European Geosciences Union.

Abstract

Mesoscale eddies seem to play an important role for both the hydrography and biogeochemistry of the eastern tropical Pacific Ocean (ETSP) off Peru. However, detailed surveys of these eddies are not available, which has so far hampered an in depth understanding of their implications for nutrient distribution and biological productivity. In this study three eddies along a section at 16° 45′ S have been surveyed intensively during R/V *Meteor* cruise M90 in November 2012. A coastal mode water eddy, an open ocean mode water eddy and an open ocean cyclonic eddy have been identified and sampled in order to determine both their hydrographic properties and their influence on the biogeochemical setting of the ETSP. In the thermocline the temperature of the coastal anticyclonic eddy was up to 2 °C warmer, 0.2 more saline and the swirl velocity was up to 35 cm s^{-1}. The observed temperature and salinity anomalies, as well as swirl velocities of both types of eddies were about twice as large as had been described for the mean eddies in the ETSP and the observed heat and salt anomalies (AHA, ASA) show a much larger variability than the mean AHA and ASA. We found that the eddies contributed significantly to productivity by maintaining pronounced subsurface maxima of chlorophyll. Based on a comparison of the coastal (young) mode water eddy and the open ocean (old) mode water eddy we conclude that the aging of eddies when they detach from the coast and move westward to the open ocean considerably influences the eddies' properties: chlorophyll maxima are weaker and nutrients are subducted. The coastal mode water eddy was found to be a hotspot of nitrogen loss in the OMZ, whereas, the open ocean cyclonic eddy was of negligible importance for nitrogen loss. Our results show that the important role the eddies play in the ETSP can only be fully deciphered and understood through dedicated high spatial and temporal resolution oceanographic/biogeochemical surveys.

BGD

10, 9179–9211, 2013

Title Page

Abstract | Introduction

Conclusions | References

Tables | Figures

◄| |►

◄ ►

Back | Close

Full Screen / Esc

Printer-friendly Version

Interactive Discussion

1 Introduction

During the last two decades nonlinear mesoscale features of the oceanic circulation (so called eddies) have been recognized to play an important role for the vertical and horizontal transport of momentum, heat, mass and the chemical constituents of seawater, such as oxygen, nutrients etc. (e.g. Klein and Lapeyre, 2009). Three types of eddies have been identified: cyclonic, anticyclonic and mode water eddies (e.g. McGillicuddy Jr. et al., 2007). It is noted that the direction of rotation of mode water eddies is the same as of anticyclonic eddies. Cyclonic eddies (cyclones) and mode water eddies can inject nutrients from below the euphotic zone into the euphotic zone while anticyclonic eddies (anticyclones) tend to decrease the nutrient content of the euphotic zone (e.g. Klein and Lapeyre, 2009). The enhanced upwelling of nutrients into the euphotic zone by eddies (i.e. eddy pumping) is especially important for the biological productivity of the oligotrophic regions of the oceans (McGillicuddy Jr. et al., 1998, 2007; Oschlies and Garcon, 1998). Only recently, however, Gruber et al. (2011) suggested that the occurrence of eddies in coastal upwelling regions, which are characterized by a high productivity, may result in a reduction of biological production.

Marine primary production is governed by temperature, light, and limiting nutrients, most notably nitrogen (N), phosphorus (P), silicon (Si) and iron (Fe) depending on plankton species. A fraction of the biologically produced particulate matter subsequently sinks into the subsurface ocean where it is consumed by microbes and macrofauna, releasing carbon dioxide (CO_2) and nutrients back to the water column and consuming subsurface O_2 (Doney, 2010). In case of slow rates of water renewal in subsurface layers this leads to low oxygen concentrations and as increasing CO_2 leads to lower pH values (e.g. Feely et al., 2008) the low oxygen waters also become increasingly “acidified” and more corrosive to carbonates.

The coastal upwelling region of Peru belongs to the four major eastern boundary upwelling systems and thus shows an overall very high biological production (e.g. Chavez and Messié, 2009). The upwelling is fed by nutrient-rich/oxygen-depleted waters of the

BGD
10, 9179–9211, 2013

poleward flowing Peru-Chile Undercurrent (Brink et al., 1983; Huyer et al., 1991). The Peruvian upwelling is adjacent to the oxygen minimum zone (OMZ) in the eastern tropical South Pacific Ocean (ETSP), which is one of three major oxygen minimum zones of the global ocean (Karstensen et al., 2008; Paulmier and Ruiz-Pino, 2009). The oxygen (O_2) concentrations in the OMZ of the ETSP are generally very low ($< 20\,\mu mol\,L^{-1}$), thus it is also an oceanic region where a significant microbial loss of fixed nitrogen (Codispoti, 2007; Gruber, 2008) (i.e. bioavailable nitrogen mainly in the form of inorganic nitrogen containing nutrients) via denitrification (reduction of nitrate via nitrite to dinitrogen), anammox (anaerobic oxidation of ammonium with nitrite to dinitrogen) and DNRA (dissimilatory nitrate reduction to ammonium) takes place (Thamdrup et al., 2012; Lam et al., 2009).

On the basis of 15 yr of satellite altimetry measurements an analysis of the mean eddy properties offshore the Peruvian coast showed that eddies are highly abundant off Peru, most frequently observed off Chimbote (9° S) and south of San Juan (15° S) (Chaigneau et al., 2008). The highest eddy frequency was found between 15° S and 18° S east of 90° W. In recent studies, measurements of three anticyclonic eddies in the eastern tropical South Pacific Ocean were performed. Two of them featured depressed near-surface isopycnals whereas one exhibited doming isopycnals (Holte et al., 2013). An anticyclonic eddy described off central-southern Chile (Morales et al., 2012) showed the typical mode water eddy distribution.

In the eastern tropical Pacific Ocean the zonal tropical current bands supply oxygen rich waters to the OMZ (Stramma et al., 2010b). In contrast, the mid-depth circulation in the eastern South Pacific is sluggish in the region of the OM and as the mean currents are weak, eddy variability strongly influences the flow and ultimately supplies oxygen-poor water to the OMZ (Czeschel et al., 2011). Model results support the view that eddies are responsible for the redistribution of oxygen within the OMZ and for the oxygen transport at the poleward boundary of the OMZ (N. Gruber, personal communication, 2012). Mesoscale variability occurs in the form of linear Rossby waves and as nonlinear vortices or eddies. In contrast to linear waves, nonlinear vortices can transport

BGD
10, 9179–9211, 2013

momentum, heat, mass and the chemical constituents of seawater, and therefore contribute to the large scale water mass distribution (e.g. Chelton et al., 2007). The degree of nonlinearity of a mesoscale feature is characterized by the ratio of the rotational fluid speed U to the translation speed c of the feature. When $U/c > 1$, the feature is nonlinear, which allows it to maintain a coherent structure as it propagates (e.g. Flierl 1981; Chelton et al., 2011).

By combining historical records of Argo float profiles and satellite data the three-dimensional eddy structure of the eastern South Pacific Ocean was described for temperature, salinity, density and velocity fields of cyclonic and anticyclonic eddies (Chaigneau et al., 2011). The core of cyclonic eddies is centered at ~ 150 m while the core of anticyclonic eddies is located at ~ 400 m depth. These differences are attributed to their formation mechanisms as cyclonic eddies are formed by instabilities of the equatorward coastal surface currents, whereas the anticyclonic eddies are likely released from the poleward subsurface Peru–Chile Undercurrent (Chaigneau et al., 2011). The mean radius of the eastern South Pacific eddies was estimated to be 122 ± 30 km (Chaigneau et al., 2011). The high eddy activity in austral spring (October to November) near 15° S coincides with areas of reduced upwelling and an important inshore advection of warmer and saltier subtropical water from 9° S to 16° S (Chaigneau et al., 2008).

Correa-Ramirez et al. (2012) suggested that the observed seasonal discrepancy between the occurrence of the max. upwelling (in austral winter) and satellite observation of the maximum chlorophyll concentrations (in austral summer) in the coastal area of Peru may be caused by an intensification and seasonal displacement of eddy kinetic energy associated with eddies north of 20° S. Moreover, coastal eddies off Peru have been shown to be sites of significant loss of fixed nitrogen (Altabet et al., 2012). Therefore, eddies off Peru seem to play an important role for biological productivity and the nitrogen cycle. However, our knowledge is mainly based on model studies and satellite observations but actual (i.e. in-situ) hydrographic and biogeochemical features of the eddies off Peru are largely unknown. Here we present the results of a first detailed survey of hydrographic and biogeochemical parameters of three eddies off Peru in order to elucidate their role for the biogeochemical cycling in the ETSP.

2 Observational data

Cruise M90 on the German research vessel R/V *Meteor* took place in November 2012 to investigate the factors controlling the intensity and areal extent of the OMZ of the eastern tropical Pacific Ocean. The cruise started in Cristobal, Panama, on 29 October and ended on 28 November in Callao, Peru. Starting on 15 November a former World Ocean Circulation Experiment (WOCE) section along 16° 45′ S was reoccupied by following an eastward cruise track from 87° W to the coast of Peru. On the basis of satellite sea level height anomaly images forwarded to the ship and which revealed two major anticyclonic eddies and one cyclonic eddy along the section (Fig. 1), a detailed survey of these eddies including acoustic Doppler current profiling (ADCP), measurements of conductivity/temperature/depth (CTD), and of major biogeochemical parameters (O_2, nutrients, chlorophyll, turbidity and pH) along several additional subsections across the eddies have been performed (Fig. 1).

Two ADCP systems recorded the ocean velocities: a hull mounted RDI OceanSurveyor 75 kHz ADCP provided the velocity distribution to about 700 m depth, while a 38 kHz ADCP mounted in the sea-well provided velocity profiles down to about 1200 m depth. Given that the eddies are centered in the upper ocean the data shown in this study for the upper ocean are exclusively from the 75 kHz ADCP, which has a higher resolution in the upper ocean. The 38 kHz ADCP data are used to determine the swirl velocities below 700 m depth.

A Seabird CTD system with a GO rosette with 24 10 L-water bottles was used for water profiling and discrete water sampling. The CTD system was used with double sensors for temperature, conductivity (salinity) and oxygen. The CTD oxygen sensor was calibrated with oxygen measurements obtained from discrete samples from the rosette applying the classical Winkler titration method using a non-electronic

BGD
10, 9179–9211, 2013

titration stand (Winkler, 1888; Hansen, 1999). The precision of the oxygen titration was $\pm 0.45\,\mu mol\,L^{-1}$. The uncertainty of the CTD oxygen sensor calibration was determined as a r.m.s. of $\pm 0.68\,\mu mol\,O_2\,kg^{-1}$. However, with the classical titration method we were not able to determine oxygen concentrations below about $2\,\mu mol\,kg^{-1}$ and hence oxygen concentrations below about $2\,\mu mol\,kg^{-1}$ could not be measured with the CTD oxygen sensor. Turbidity given in NTU (Nephelometric Turbidity Units) and chlorophyll concentrations ($\mu g\,L^{-1}$) were measured with a WetLabs FLNTU instrument attached to the CTD. We used the original calibration provided by the company with sensitivities of 0.01 NTU and $0.025\,\mu g\,L^{-1}$ but did not apply any shipboard calibration and hence the measured absolute values may have a somewhat larger uncertainty, but the gradients determined across the eddies are clearly reliable.

Nutrients were measured on-board with a QuAAtro auto-analyzer (Seal Analytical). Nitrite (NO_2^-), nitrate (NO_3^-), phosphate (PO_4^{3-}) and silicate (SiO_2) were measured with a precision of $\pm 0.1\,\mu mol\,L^{-1}$, $\pm 0.1\,\mu mol\,L^{-1}$, $\pm 0.02\,\mu mol\,L^{-1}$ and $\pm 0.24\,\mu mol\,L^{-1}$, respectively. N^* was calculated as $N^* = (NO_3^- + NO_2^-) - 16PO_4^{3-}$ (see Altabet et al., 2012 and references therein).

The pH measurements were carried out with a Mettler Toledo potentiometer, model SevenGo, with an InLab 413 SG IP67 electrode calibrated with buffer solutions at pH values 4, 7 and 10.

Anomalies were calculated as the difference between concentrations measured at the stations at the edge of the eddy and those in its center. The locations chosen for comparison are marked in the figures representing each section. The available heat anomalies (AHA) and available salt anomalies (ASA) were computed as described in Chaigneau et al. (2011).

Aviso satellite derived altimeter sea surface height anomaly data (SSHA) were used to define the general distribution of eddies and to identify their individual spacial extent during the cruise. The SSHA data used in this study are delayed time products and combine available data of all satellites. The data are resampled on a regular 0.25° grid and are calculated with respect to a seven-year mean (http://www.aviso.oceanobs.

BGD
10, 9179–9211, 2013

com). MODIS-aqua satellite derived chlorophyll data were used for a better visualization of the distribution of chlorophyll at the surface of the coastal eddy. The chlorophyll data provided by the Giovanni data portal (http://disc.sci.gsfc.nasa.gov/giovanni/additional/users-manual), are averaged for each grid cell over a time range of 8 days with a resolution of 1/24°.

3 Results

3.1 The anticyclonic eddies

Several anticyclonic (counter-clockwise rotation in the Southern Hemisphere) features were clearly visible in the SSHA data in the region off Peru at the time of Cruise M90 in November 2012 (Fig. 1). Along the 16° 45′ S section one anticyclonic eddy (eddy B) was centered in the open ocean at about 17° S, 83° W and another anticyclonic eddy (eddy A) was centered close to the shelf at about 16° S, 76° W. These two features offered the possibility to compare a young eddy (i.e. eddy A) formed near the shelf with an older open ocean eddy (i.e. eddy B).

3.2 The formation region (eddy A)

Anticyclonic eddy A had already separated from the shelf in late November 2012. An overview of the measured velocity and parameter distributions shows the opposing directions of the flow and the corresponding velocities of the anticyclonic circulation and the oxygen minimum core in the center of the eddy where the velocity components change direction (Fig. 2). The largest anomalies were observed in the upper 600 m but the anticyclonic velocity components were still seen at the greatest depths reached with the shipboard ADCP at about 1200 m. As described for other anticyclonic eddies (Chaigneau et al., 2011), the highest meridional speed occurred between 50 m and 250 m depth. The density distribution shows a deepening of the isopycnals below 110 m and an uplift above 110 m which is typical for a mode-water eddy (McGillicuddy Jr.

BGD
10, 9179–9211, 2013

et al., 2007). Connected to the uplift of the isopycnals, the anticyclonic swirl velocity derived as the mean of maximum positive and negative velocity perpendicular to the section used at each depth decreased above 110 m (Fig. 3). The corresponding salinity and temperature was elevated in the center of the eddy (Chaigneau et al., 2011). The anticyclone off the shelf showed a temperature increase of 2 °C and a salinity increase of 0.2 in its core (Fig. 3), which is about twice as large as that of mean anticyclones in the eastern tropical South Pacific (Chaigneau et al., 2011). Also the observed swirl velocity of up to 35 cm s^{-1} is more than twice and up to three times as high as for the mean anticyclones.

Given that oxygen is generally low below 30–50 m water depth in the eastern tropical Pacific only a weak further reduction in oxygen is possible. Nevertheless the oxygen minimum linked to the eddy is clearly visible in the section across the eddy (Fig. 2). There is a pronounced decrease of the oxygen concentrations by more than 200 µmol kg^{-1} from the surface to 50 m depth (Fig. 3) where the uplift of the near surface isopycnals led to a significant shoaling of the mixed layer. Nitrate was reduced at 100–300 m depth by ~ 20 µmol L^{-1} and nitrite increased at 100–400 m depth. A pronounced increase in phosphate and silicate concentration was observed between 50 m and 150 m depth. Turbidity was higher at about 50–400 m depth and the pH was generally higher between 100 m and 400 m depth but displayed the highest decreasing gradient from the surface down to around 50 m depth (Fig. 3). The chlorophyll distribution in the upper ocean was characterized by a very large chlorophyll maximum near 50 m depth for the center of the anticyclone (Fig. 4) connected to a positive turbidity anomaly of 0.1 NTU (Fig. 3). The increased chlorophyll values near the surface at 76.6° W to 76.7° W were related to high near coastal chlorophyll values, which were visible in chlorophyll satellite images taken at the end of November 2012 (Fig. 5) and which were transported offshore at the northern rim of the anticyclone.

According to sea level anomaly images this anticyclone was formed after 13 September 2012 and stayed near the coast until mid-November 2012. The anticyclone was centered at 76° W on 21 November 2012, then moved westward in December and

BGD
10, 9179–9211, 2013

could be tracked to 81° W at 25 March 2013. The westward movement of 5 degrees in 100 days translates into a westward transit speed of $6.1\,\mathrm{cm\,s^{-1}}$.

The vertical extent of the eddy is defined where the swirl velocity or rotational speed is larger than the translation speed ($U/c > 1$). For the mean anticyclonic eddies between 10° S and 20° S the vertical extent was 450 m (Chaigneau et al., 2011). The two anticyclonic eddies subject to our study had a vertical extent of more than 600 m, however, we carried out the anomaly computation to 600 m depth only (Table 1). The volume of anticyclone A was $5.2 \times 10^{12}\,\mathrm{m^3}$, similar to the volume of $4.9 \times 10^{12}\,\mathrm{m^3}$ of the mean anticyclone. However, the AHA of 17.7×10^{18} J and the ASA of 36.5×10^{10} kg are a factor 2.7 and 2.1 larger than for the mean anticyclone, respectively, based on their larger vertical extent and higher temperature and salt anomalies.

The section A2 along 16° 45′ S that changed to northeasterly direction towards the shelf at 76° W (Fig. 6) crossed the southern part of anticyclonic eddy A (Fig. 1). It documents the isolated low oxygen core of the eddy and the low oxygen core right at the shelf. Salinity, temperature and density again showed the signature of the mode-water type eddy and upwelling in the upper 150 m near the shelf (Fig. 6, left). The meridional velocity distribution clearly shows that this eddy was separated already from the coast given that near the shelf the southward flowing Peru–Chile Undercurrent flows in the opposite direction as the flow component in the eastern part of the anticyclone, which is directed northward.

High resolution profiles of bottle samples for nutrient determination were only taken east of 76° W for this section A2 (Fig. 6, right). As a function of upwelling intensity the nitrite layer rose near the shelf and higher nitrate, phosphate and silicate concentrations were located near the surface. Nitrite concentrations levels near the shelf and in the anticyclone at 50 m to 400 m depth were very high as a consequence of the productive shelf waters off Peru having the highest nitrogen transformation rates due to anammox processes (Kalvelage et al., 2013).

3.3 The open ocean region (eddy B)

The parameter distribution in the anticyclonic eddy B centered in the open ocean at about 83° 50′ W at 16° 45′ S shows the low oxygen layer extending vertically between 100 and 600 m depth (Fig. 7). The open ocean anticyclonic eddy was a weak mode water type anticyclone with the change in density anomaly occurring at 300 m depth. Below 200 m depth salinity and temperature anomalies were positive and oxygen anomalies were slightly negative. Between 100 m and 200 m depth strong negative salinity, temperature and oxygen anomalies are present (Fig. 3). Distinct maxima of phosphate, silicate and nitrate concentration anomalies were located at 120 m to 150 m depth. Similar to near-shelf anticyclone A, turbidity was higher in the eddy between 50 m and 400 m, however, without the enhanced maximum below the mixed layer. The chlorophyll section shows a maximum in the core of the eddy (Fig. 4) much weaker than in the coastal anticyclone. As the mixed layer reached deeper, enhanced chlorophyll values reach down to about 80 m depth and hence deeper than for the coastal anticyclone A. The swirl velocity at 200 to 400 m depth was much weaker than for the coastal anticyclone A. The maximum swirl velocities of 16 $cm\,s^{-1}$ are about twice as large as for the mean anticyclones (Chaigneau et al., 2011).

In comparison with the coastal anticyclone A, the anomalies observed in the oxygen minimum zone are weaker below about 200 m depth in the open ocean anticyclone B, especially for temperature and density. The anomalies below the mixed layer were similar for temperature, oxygen, phosphate and silicate, however located about 100 m deeper in the open ocean eddy than near the coast.

Following the trajectory of the anticyclone B back in time it was located at 78° 15′ W on 7 August 2012. Hence the anticyclone moved 570 km westward in 100 days corresponding to a westward propagation speed of 6.5 $cm\,s^{-1}$, which is only slightly faster than the westward movement of the coastal anticyclone A.

Although the vertical extent of eddy B of more than 600 m was again larger than that of the mean eddy (Table 1) the volume of $4.7 \times 10^{12}\,m^3$ was slightly less than that of

BGD
10, 9179–9211, 2013

the mean eddy as the radius defined between the maxima in swirl velocities was a little smaller. The AHA was only half of the mean anticyclonic eddy as the temperature anomaly was negative in the upper 200 m for the mode water type eddy while the ASA was similar to the mean anticyclone.

3.4 The cyclonic feature (eddy C)

Several cyclonic (clockwise rotation in the Southern Hemisphere) features were visible in the region off Peru at the time of the R/V *Meteor* cruise in November 2012 (Fig. 1). Along the 16° 45′ S section a large cyclonic eddy (i.e. eddy C) was centered at about 81° W on 21 November 2012 with a strong southwest to northeast extension.

Cyclones dome for both the mixed layer and the main thermocline as corroborated by a positive density anomaly for the entire 600 m shown (Figs. 3 and 8). The swirl velocity core of cyclones is expected near the surface and the cyclone at 81° W accordingly had the largest velocities of about 30 cm s^{-1} at about 50 m depth. The parameter distribution on the diagonal section C between 15° 10′ S and 17° 30′ S shows elevated oxygen concentrations in the OMZ centered at 16° 30′ S corresponding to higher pH values (Fig. 8). No nitrite was observed in the core of cyclone C, while the nitrite maximum found in the southern part of the section (Fig. 8) originated from a neighboring anticyclonic eddy located at the southern end of the section (Fig. 1). Salinity and temperature decreased by 0.3 and up to 2 °C, respectively, which is again about twice as much as that of the mean cyclones (Chaigneau et al., 2011; Fig. 5), as well as of a cyclonic eddy measured in November 2008 in the eastern Pacific (Subramanian et al., 2013). The temperature, salinity, density and silicate anomalies of cyclone C in the OMZ were of similar strength as those of the coastal anticyclone A, but with opposite sign. The oxygen anomaly of the cyclone C was even larger in the OMZ than observed for the coastal anticyclone, which is explained by the fact that in the OMZ it is easier to create an anomaly by adding high oxygen waters than to reduce very low oxygen levels further.

Below the mixed layer at about 100 m depth the oxygen anomaly was lowest due to the uplift of the main thermocline but phosphate and silicate only show weak positive anomalies at about 80 m and weak negative anomalies at about 130 m (Fig. 3). A chlorophyll maximum was located between 20 and 40 m depth slightly to the north of the core of the cyclonic eddy C. This chlorophyll maximum was higher than that of anticyclone B in the open ocean and showed a higher positive turbidity anomaly in the upper 40 m.

Cyclonic eddy C appeared in September 2012 at the coast at 16° S, 76° W and immediately moved westward without staying attached to the shelf. This cyclone reached 81° W on 21 November, which corresponds to a westward transit speed of 7.9 cm s^{-1}. As can be seen in the sea level anomaly distribution (Fig. 1) the cyclonic eddy C had a wider core and only a weak maximum at 81° W, hence the core of the eddy may have been located further to the east, which would reduce the calculated westward transit speed. However, tracking the eddy forward in time showed that its core reached 85° W on 13 February 2013 which results in a westward velocity of 7.4 cm s^{-1}.

While the vertical extent of the mean cyclonic eddy was only 200 m, that of eddy C reached again deeper to 950 m depth (not shown) and also the radius of 88 km was much larger than the 62.3 km for the mean cyclonic eddy (Table 1). Therefore, the AHA of eddy C for the upper 600 m was 8.4 times and the ASA 6.7 times larger than for the mean cyclonic eddy. However, the cyclonic feature C is quite unusual given its elongated shape and should not be considered the typical cyclonic eddy.

4 Discussion

The depth distributions of the temperature and salinity anomalies based on detailed CTD sections and the swirl velocity derived from the ADCP measurements of the eddies A–C are in agreement with the mean fields derived from float profiles (Chaigneau et al., 2011). However, as mentioned above the temperature and salinity anomalies and the swirl velocity obtained from our in-situ measurements along 16° 45′ S are up to

BGD
10, 9179–9211, 2013

2 °C warmer, 0.3 more saltier and more than twice as large (up to 35 cm s^{-1}), respectively, as those computed for the mean eastern South Pacific eddies (Chaigneau et al., 2011). The large temperature and salinity anomalies might be caused by using the actual measured values instead of a climatology as reference for the parameter distribution outside of the eddies as used by Chaigneau et al. (2011). The lower swirl velocity computed by Chaigneau et al. (2011) is caused by their assumption of a level of zero velocity at 1000 m depth for the mean distribution while in our study the deep reaching measurements using the 38 kHz ADCP showed a swirl component of 7.5 cm s^{-1} for eddy A, 7.7 cm s^{-1} for eddy B and 6.8 cm s^{-1} for eddy C at 1000 m depth.

After its formation anticyclonic eddy A stayed attached to the shelf for about 2 months before it began to move westward in December 2012. The westward transit speed of the eddies B and C were estimated for 3.5 months and 3 month time periods, respectively. The estimated westward transit speeds for the eddies A–C were in the range from 6.1 cm s^{-1} (eddy A) to 7.9 cm s^{-1} (eddy C). Hence they are slightly higher than the mean westward eddy propagation speed of 3–6 cm s^{-1} computed for the region off Peru (Chaigneau et al., 2008). This discrepancy is probably due to the fact that our measurements in the northern reaches of the westward flowing subtropical gyre (Kessler, 2006).

We observed pronounced maxima and minima for the majority of the hydrographic (temperature, salinity, density) and biogeochemical (nutrients, oxygen, turbidity, pH) anomalies in 50 m and 150 m depth of the coastal eddy A and the open ocean eddy B, respectively (Fig. 3). These characteristic anomalies most likely originated from the nutrient-enriched/oxygen-depleted Peru–Chile Undercurrent (PCU) which flows poleward in in a depth range from 50 to 350 m and which prevails at distances between 65 and 165 km from the Peruvian coast (Huyer et al., 1991). The PCU fuels the coastal upwelling of Peru (Brink et al., 1983; Huyer et al., 1991). During the wind-driven upwelling the waters of the PCU are brought to the surface at the shelf (Fig. 6). However, the uplifted nutrient-rich/oxygen-depleted water of the Peru–Chile Undercurrent was trapped in upper part of eddy A when it was detached from the shelf. Obviously the anomalies are generally weakening and are subducted to 150 m when an eddy is aging while moving westward as can be seen for eddy B (Fig. 3). The only exception is the NO_3^- anomaly which does not show a maximum at 50 m (eddy A) or 150 m depth (eddy B). This is caused by the fact that the trapped PCU is enriched in nutrients except NO_3^- because in low oxygen waters denitrification and/or DNRA lead to a decrease of NO_3^- concentrations. The pronounced subsurface chlorophyll maxima in the eddies A–C that were found in a depth range from 30 m (eddy C) to 50 m (eddy A, Fig. 4), are a typical feature of both cyclonic and mode water eddies, which is caused by eddy pumping of nutrients into the euphotic zone (see e.g. McGillicuddy et al., 1998, 2007). The eddy pumping results from the uplift of the isopycnals in the core of eddies A–C (see Figs. 2, 7 and 8). Comparison of the chlorophyll maxima of the "young" coastal eddy A and the "older" open ocean eddies B and C reveals that the chlorophyll concentrations in the subsurface maxima are significantly lower in the eddies B and C because of decreasing eddy pumping (i.e. less pronounced uplift of the isopycnals, see Figs. 7 and 8) while the eddies were moving westward.

The chlorophyll concentrations of the subsurface maximum in eddy A are in the same concentration range as the chlorophyll concentrations in the surface layer of the coastal upwelling (see Fig. 4). Assuming that chlorophyll concentrations can be taken as a (qualitative) indicator for primary productivity this finding suggests that mesoscale eddies off the coast of Peru contribute significantly to overall productivity. Additionally, the development of a pronounced filament structure at the northern fringe of eddy A (which is clearly visible in the satellite picture, see Fig. 5) documents that due to the rotation of the eddy, highly productive surface waters are transported westward far beyond the narrow band of coastal upwelling at the shelf.

Both the vertical concentration distributions (Fig. 2), as well as the anomalies (Fig. 3) of oxygen and nutrients (i.e. nitrate, nitrite) in mode water eddy A reveal a core layer where pronounced loss of fixed nitrogen occurs. This is indicated by the pronounced maximum of NO_2^- concentrations (often also referred to as the secondary nitrite maximum, SNM) at about 250–300 m depth, which is associated with the pronounced

BGD
10, 9179–9211, 2013

minima of both O_2 ($< 5\,\mu mol\,L^{-1}$) and NO_3^- concentrations between 100 and 300 m depth. Please note that the OMZ (here defined as $O_2 < 20\,\mu mol\,L^{-1}$) spreads from 100 to 600 m depth. The co-occurrence of extremely depleted O_2 and NO_3^-, coinciding with high NO_2^- concentrations have been attributed to on-going denitrification (Fiadeiro and Strickland, 1968; Codispoti et al., 1986) or DNRA (Lam et al., 2009). Enhanced turbidity as a measure for suspended material and particles, is also found between 100 and 300 m in eddy A (Fig. 3) which indicates the existence of an intermediate nepheloid layer known to be associated with enhanced microbial activity. These layers are, moreover, known to play important roles in other OMZs adjacent to coastal upwelling regions such as the Arabian Sea and off NW Africa (Naqvi et al., 1993; Fischer et al., 2009).

A similar feature is seen in the O_2 and NO_2^-/NO_3^- distributions and anomalies (Figs. 3 and 7) of the mode water eddy B. However, the maximum concentration of NO_2^- of up to $5\,\mu mol\,L^{-1}$ measured in eddy B is significantly lower than that of up to $11\,\mu mol\,L^{-1}$ measured in eddy A. This points to a significantly lower activity of nitrogen loss processes in eddy B. The NO_2^- concentrations measured during our cruise in November 2012 are in the same range as those reported in previous studies of the SNM in the OMZ off Peru (see e.g. Barber and Huyer, 1979; Copin-Montégut and Raimbault, 1994; Altabet et al., 2012) but lower than the exceptionally high NO_2^- concentrations (up to $23\,\mu mol\,L^{-1}$ in February/March 1985) reported by Codispoti et al. (1986).

In contrast to the mode water eddies A and B, the core of cyclonic eddy C shows a compression of the OMZ to a narrow band between 150–450 m where no loss of NO_3^- and no enhanced NO_2^- concentrations have been measured. Signs of nitrogen loss processes in eddy C are only visible at the southern fringe at about 17° S (Fig. 8) which are caused by an adjacent anticyclonic eddy (Fig. 1). Thus, we conclude that in eddy C active nitrogen loss processes were negligible at the time of our measurements.

N* (for a definition see the section on observational data) is an indicator for nitrogen sink/source processes in the water column: negative N* values indicate nitrogen sinks

BGD
10, 9179–9211, 2013

including denitrification, DNRA and anammox, whereas, positive N* values indicate nitrogen sources such as N_2 fixation. The vertical distribution of the N* anomalies (ΔN*, Fig. 3) show well defined ΔN* minima of about $-35\,\mu mol\,L^{-1}$ in 50 m depth (eddy A) and of about $-20\,\mu mol\,L^{-1}$ in 150 m depth (eddy B). Moreover, a second, even broader, ΔN* minimum of about $-20\,\mu mol\,L^{-1}$ at about 200 m is visible in eddy A, but there is no second ΔN* minimum detectable in eddy B although ΔN* remains slightly negative. Following the arguments of Altabet et al. (2012), we attribute the second ΔN* minimum in eddy A and the negative ΔN* in eddy B to active nitrogen loss processes within eddies of the OMZ. The upper ΔN* minimum, which is located above the OMZ, is most probably a residual of the uplifted PCU during its upwelling at the shelf. This is in contrast to the interpretations of Altabet et al. (2012) who argued that the upper N* minimum observed in a comparable anticyclonic coastal eddy off Peru resulted from shelf waters that had been in contact with shelf sediments and thus were carrying signals of sedimentary dentrification and/or anammox (Altabet et al., 2012).

The decreased ΔN* values of eddy B compared to those in eddy A points to a decline of the nitrogen loss processes during aging of mode water eddies on their way from the coast to the open ocean. In sharp contrast to eddies A and B, the vertical distribution of ΔN* (Fig. 3) shows positive values in the OMZ (150–450 m). However, these data cannot be interpreted as being caused by enhanced nitrogen sources but resulted from the fact that N* at the fringes of the cyclonic eddy C (see e.g. NO_2^- distribution in Fig. 8), which are influenced by an adjacent, anticyclonic eddy, were more negative than those in the core of eddy C.

Recently, concern has emerged that CO_2-driven climate change results in decreasing dissolved oxygen (DO) levels in the ocean (e.g. Keeling and Garcia, 2002; Bopp et al., 2002) with potentially large impacts on marine habitats and ecosystems (Keeling et al., 2010; Stramma et al., 2012b). Continuous time series in a few selected tropical areas with sufficient data (Stramma et al., 2008), as well as comparison between two distinct time periods in the tropical oceans (Stramma et al., 2010a), and observed changes at 300 dbar for the entire ocean over the past 50 yr (Stramma et al., 2012a)

BGD
10, 9179–9211, 2013

indicate an ongoing decline of oxygen and a vertical expansion of the OMZ in most tropical regions, contrasted by areas dominated by DO increase, predominantly in the subtropical gyres. However, Chaigneau et al. (2009) computed a decreasing trend for the number of generated eddies off Peru and Chile in the period 1995–2007. Assuming that this trend is continuing we speculate that a decreasing number of eddies might lead to an increase of the oxygen concentrations in the OMZ off Peru: a decreasing eddy-fueled productivity will lead to a decreasing transport of organic material to the open ocean which, in turn, decrease the demand of oxygen for respiration. Decreasing numbers of eddies might also influence the number of nitrogen loss hotspots, thus the total nitrogen loss from the ETSP might be decreasing in the future if the decreasing trend in numbers of eddies will continue.

Fundamental to a realistic prediction of changing future OMZs are, however, accurate determinations of oxygen distributions, processes maintaining the OMZ, and dynamics of the OMZ, of which eddies may be one of the most important components.

5 Conclusions

Two mode water eddies and one cyclonic eddy (see eddies A–C in Fig. 1) were investigated in detail along a cruise track at 16° 45′ S off Peru in November 2012 in order to determine both the hydrographic properties and the influence of eddies on the biogeochemical cycling of the ETSP. The motivation of this study arose from the fact that detailed information on the oxygen and nutrient anomalies in eddies had not been reported previously for the eastern tropical South Pacific Ocean.

In the thermocline the temperature of the coastal anticyclonic eddy was up to 2 °C warmer, 0.2 more saltier and the swirl velocity was up to $35\,\mathrm{cm\,s^{-1}}$. The observed temperature, salinity anomalies and swirl velocities of both types of eddies were about twice as large as had been described for the mean eddies in the ETSP. The AHA and ASA estimates for the upper 600 m showed that eddies are quite variable leading to large deviations from the mean state. The vertical extent of the mean eddies might

Discussion Paper | Discussion Paper | Discussion Paper | Discussion Paper |
BGD
10, 9179–9211, 2013
Biogeochemistry anomalies in eddies off Peru
L. Stramma et al.

be biased to low values due to the chosen zero reference velocity at 1000 m depth, which contrasts with our direct measurements showing the eddy swirl velocity to reach deeper than 1000 m at values of about 7 $cm\,s^{-1}$ at 1000 m depth.

Based on our data we conclude that young coastal eddies significantly contribute to productivity off Peru by the development of productivity maxima in the subsurface, which are fueled by nutrient-rich upwelled waters originating from the PCU trapped in coastal eddies. However, the subsurface productivity decreases when both mode water and cyclonic eddies are detached from the coast and move westward. The aging of the mode water eddies is associated with a significant subduction of nutrients within the eddies from 50 to 150 m which suggests that mode water eddies may reduce the adjacent open ocean productivity off Peru. This finding supports the model results from Gruber et al. (2011). In the core of the coastal mode water eddy pronounced and active nitrogen loss took place. However, the nitrogen loss was considerably lower in the older, open ocean mode water eddy. Moreover, the surveyed open ocean cyclonic eddy did not show any significant active nitrogen loss. Thus, we conclude that coastal mode water eddies are indeed a hotspot of nitrogen loss off Peru as proposed by Altabet et al. (2012). However, the open ocean mode water eddy and the cyclonic eddy seem to be of reduced importance or even negligible, respectively, as hotspots of active nitrogen loss. This may be caused by the reduced flux of organic matter, as indicated by the decrease of the chlorophyll maxima in the open ocean eddies.

Our results indicate that eddies play an important role for the hydrographic setting and biogeochemical cycling of the ETSP. The comparably small scale temporal and spatial variability associated with eddies should be taken into accounted in future oceanographic/biogeochemical surveys in the area.

Acknowledgements. The Deutsche Forschungsgemeinschaft (DFG) provided support as part of the “Sonderforschungsbereich 754: Climate–Biogeochemistry Interactions in the Tropical Ocean” (LS, HWB, RC, MF). Additional support was provided through the Instituto del Mar del Peru, IMARPE (AL). We thank G. Krahmann, T. Fischer, M. Lohmann and T. Baustian for providing measurements and final processing of the various data sets presented. The altimeter data were produced by Ssalto/Duacs and distributed by Aviso with support from

Cnes. Analyses and visualizations of chlorophyll used in this study were produced with the Giovanni online data system, developed and maintained by the NASA GES DISC. We also acknowledge the MODIS mission scientists and associated NASA personnel for the production of the data used in this research effort. We thank the authorities of Peru for the permission to work in their territorial waters.

The service charges for this open access publication have been covered by a Research Centre of the Helmholtz Association.

References

Altabet, M. A., Ryabenko, E., Stramma, L., Wallace, D. W. R., Frank, M., Grasse, P., and Lavik, G.: An eddy-stimulated hotspot for fixed nitrogen-loss from the Peru oxygen minimum zone, Biogeosciences, 9, 4897–4908, doi:10.5194/bg-9-4897-2012, 2012.

Barber, R. T. and Huyer, A.: Nitrite and static stability in the coastal waters off Peru, Geophys. Res. Lett., 6, 409–412, 1979.

Brink, K. F., Halpern, D., Huyer, A., and Smith, R. L.: The physical environment of the Peruvian upwelling g system, Prog. Oceanogr., 12, 285–305, 1983.

Bopp, L., Le Quere, C., Heimann, M., Manning, A. C., and Monfray, P.: Climate induced oceanic fluxes: implications for the contemporary carbon budget, Global Biogeochem. Cy., 16, 1022, doi:10.1029/2001GB001445, 2002.

Chaigneau, A., Gizolme, A., and Grados, C.: Mesoscale eddies off Peru in altimeter records: identification algorithms and eddy spatio-temporal patterns, Prog. Oceanogr., 79, 106–119, 2008.

Chaigneau, A., Eldin, G., and Dewitte, B.: Eddy activity in the four major upwelling systems from satellite altimetry (1992–2007), Prog. Oceanogr., 83, 117–123, doi:10.1016/j.pocean.2009.07.012, 2009.

Chaigneau, A., Le Texier, M., Eldin, G., Grados, C., and Pizarro, O.: Vertical structure of mesoscale eddies in the eastern South Pacific Ocean: a composite analysis from altimetry and Argo profiling floats, J. Geophys. Res., 116, C11025, doi:10.1029/2011JC007134, 2011.

BGD
10, 9179–9211, 2013

Biogeochemistry anomalies in eddies off Peru

L. Stramma et al.

Chavez, F. P. and Messie, M.: A comparison of eastern upwelling boundary upwelling systems, Prog. Oceanogr., 83, 80–96, 2009.
Chelton, D. B., Schlax, M. G., Samelson, R. M., and de Szoeke; R. A.: Global observations of large oceanic eddies, Geophys. Res. Lett., 34, L15606, doi:10.1029/2007GL030812, 2007.
Chelton, D. B., Gaube, P., Schlax, M. G., Early, J. J., and Samelson, R. M.: The influence of nonlinear mesoscale eddies on near-surface oceanic clorophyll, Science, 334, 328–332, 2011.
Codispoti, L. A.: An oceanic fixed nitrogen sink exceeding 400 Tg N a^{-1} vs the concept of homeostasis in the fixed-nitrogen inventory, Biogeosciences, 4, 233–253, doi:10.5194/bg-4-233-2007, 2007.
Codispoti, L. A., Friederich, G. E., Packard, T. T., Glover, H. E., Kelly, P. J., Spinrad, R. W., Barber, R. T., Elkins, J. W., Ward, B. B., Lipschultz, F., and Lostaunau, N.: High nitrite levels off northern Peru: a signal of instability in the marine denitrification rate, Science, 233, 1200–1202, doi:10.1126/science.233.4769.1200, 1986.
Copin-Montegut, C. and Raimbault, P.: The Peruvian upwelling near 15° S in August 1986, results of continuous measurements of physical and chemical properties between 0 and 200 m depth, Deep Sea Res. Part I, 41, 439–467, 1994.
Correa-Ramirez, M. A., Hormazabel, S. E., and Morales, C. E.: Spatial patterns of annual and interannual surface chlorophyll *a* variability in the Peru–Chile Current system, Prog. Oceanogr., 92–95, 8–17, 2012.
Czeschel, R., Stramma, L., Schwarzkopf, F. U., Giese, B. J., Funk, A., and Karstensen, J.: Middepth circulation of the eastern tropical South Pacific and its link to the oxygen minimum zone, J. Geophys. Res., 116, C01015, doi:10.1029/2010JC006565, 2011.
Doney, S. C.: The growing human footprint on coastal and open-ocean biogeochemistry, Science, 328, 1512–1516, 2010.
Feely, R. A., Sabine, C. L., Hernandez-Ayon, J. M., Ianson, D., and Hales, B.: Evidence for upwelling of corrosive "acidified" water onto the continental shelf, Science, 320, 1490–1492, 2008.
Fiadeiro, M. and Strickland, J. D. H.: Nitrate reduction and the occurrence of a deep nitrite maximum in the ocean of the west coast of South America, J. Mar. Res., 26, 187–201, 1968.

BGD
10, 9179–9211, 2013
Biogeochemistry anomalies in eddies off Peru
L. Stramma et al.

Fischer, G., Reuter, C., Karakas, G., Nowald, N., and Wefer, G.: Offshore advection of particles within the Cape Blanc filament, Mauritania: results from observational and modelling studies, Prog. Oceanogr., 83, 322–330, doi:doi:10.1016/j.pocean.2009.07.023, 2009.
Flierl, G. R.: Particle motions in large-amplitude wave fields, Geophys. Astrophys. Fluid Dyn., 18, 39–74, 1981.
Gruber, N.: The marine nitrogen cycle: overview and challenges, in: Nitrogen in the Marine Environment, edited by: Capone, D. G., Bronk, D. A., Mulholland, M. R., and Carpenter, E. J., Elsevier, Amsterdam, 1–50, 2008.
Gruber, N., Lachkar, Z., Frenzel, H., Marchesiello, P., Münnich, M., McWilliams, J. C., Nagai, T., and Plattner, G.-P.: Eddy-induced reduction of biological production in eastern boundary upwelling systems, Nat. Geosci., 4, 787–792, doi:10.1038/NGEO1273, 2011.
Hansen, H. P.: Determination of oxygen, in: Methods of Seawater analysis, edited by: Grasshoff, K. K. and Ehrhardt, M., Wiley-VCH, Weinheim, 75–89, 1999.
Holte, J., Straneo, F., Moffat, C., Weller, R., and Farrar, J. T.: Structure and surface properties of eddies in the southeast Pacific Ocean, J. Geophys. Res., 118, 1–15, doi:10.1002/jgrc.20175, 2013.
Huyer, A., Paluszkiewic, K. M. T., and Smith, R. L.: The Peru Undercurrent: a study in variability, Deep-Sea Res., 38, Suppl. 1, 247–271, 1991.
Kalvelage, T., Lavik, G., Lam, P., Contreras, S., Arteaga, L., Löscher, C. R., Oschlies, A., Paulmier, A., Stramma, L., and Kuypers, M. M. M.: Nitrogen cycling driven by organic matter export in the South Pacific oxygen minimum zone, Nat. Geosci., 6, 228–234, doi:10.1038/NGEO1739, 2013.
Karstensen, J., Stramma, L., and Visbeck, M.: Oxygen minimum zones in the eastern tropical Atlantic and Pacific oceans, Prog. Oceanogr., 77, 331–350, 2008.
Keeling, R. F. and Garcia, H.: The change in oceanic O_2 inventory associated with recent global warming, P. Natl. Acad. Sci. USA, 99, 7848–7853, 2002.
Keeling, R. F., Körtzinger, A., and Gruber, N.: Ocean deoxygenation in a warming world, Annu. Rev. Mar. Sci., 2, 199–229, 2010.
Kessler, W. S.: The circulation of the eastern tropical Pacific: a review, Prog. Oceanogr., 89, 181–217, doi:10.1016/j.pocean.2006.03.009, 2006.
Klein, P. and Lapeyre, G.: The oceanic vertical pump induced by mesoscale and submesoscale turbulence, Annu. Rev. Mar. Sci., 1, 351–375, 2009.

BGD
10, 9179–9211, 2013

Lam, P., Lavik, G., Jenssen, M. M., Van de Vossenberg, J., Schmid, M., Woebken, D., Gutierrez, D., Amann, R., Jetten, M. S. M., and Kuypers, M. M. M.: Revising the nitrogen cycle in the Peruvian oxygen minimum zone, P. Natl. Acad. Sci. USA, 106, 4752–4757, 2009.

McGillicuddy Jr., D. J., Robinson, A. R., Siegel, D. A., Jannasch, H. W., Johnson, R., Dickey, T. D., McNeil, J., Michaels, A. F., and Knap, A. H.: Influence of mesoscale eddies on new production in the Sargasso Sea, Nature, 394, 263–266, 1998.

McGillicuddy Jr., D. J., Anderson, L. A., Bates, N. R., Bibby, T., Buesseler, K. O., Carlson, C. A., Davis, C. S., Ewart, C., Falkowski, P. G., Goldthwait, S. A., Hansell, D. A., Jenkins, W. J., Johnson, R., Kosnyrev, V. K., Ledwell, J. R., Li, Q. P., Siegel, D. A., and Steinberg, D. K.: Eddy/wind interactions stimulate extraordinary mid-ocean plankton blooms, Science, 316, 1021–1026, 2007.

Morales, C. E., Hormazabel, S., Correa-Ramirez, M., Pizarro, O., Silva, N., Fernandez, C., Anabalon, V., and Torreblanco, M. L.: Mesoscale variability and nutrient-phytoplankton distribution off central-southern Chile during the upwelling season: the influence of mesoscale eddies, Prog. Oceanogr., 104, 17–29, 2012.

Naqvi, S. W. A., Dileep Kumar, M., Narvekar, P. V., De Sousa, S. N., George, M. D., and De-Silva, D.: An intermediate nepheloid layer associated with high microbial metabolic rates and denitrification in the northwestern Indian Ocean, J. Geophys. Res., 98, 16469–16479, 1993.

Oschlies, A. and Garcon, V.: Eddy-induced enhancement of primary production in a model of the North Atlantic Ocean, Nature, 394, 266–269, 1998.

Paulmier, A. and Ruiz-Pino, D.: Oxygen minimum zones (OMZs) in the modern ocean, Prog. Oceanogr., 80, 113–128, 2009.

Stramma, L., Johnson, G. C., Sprintall, J., and Mohrholz, V.: Expanding oxygen-minimum zones in the tropical oceans, Science, 320, 655–658, 2008.

Stramma, L., Schmidtko, S., Levin, L. A., and Johnson, G. C.: Ocean oxygen minima expansions and their biological impacts, Deep-Sea Res. Part I, 57, 587–595, 2010a.

Stramma, L., Johnson, G. C., Firing, E., and Schmidtko, S.: Eastern Pacific oxygen minimum zones: supply paths and multidecadal changes, J. Geophys. Res., 115, C09011, doi:10.1029/2009JC005976, 2010b.

Stramma, L., Oschlies, A., and Schmidtko, S.: Mismatch between observed and modeled trends in dissolved upper-ocean oxygen over the last 50 yr, Biogeosciences, 9, 4045–4057, doi:10.5194/bg-9-4045-2012, 2012a.

Stramma, L., Prince, E. D., Schmidtko, S., Luo, J., Hoolihan, J. P., Visbeck, M., Wallace, D. R. W., Brandt, P., and Körtzinger, A.: Expansion of oxygen minimum zones may reduce available habitat for tropical pelagic fishes, Nat. Clim. Change, 2, 33–37, 2012b.
Subramanian, A. C., Miller, A. J., Cornuelle, B. D., Di Lorenzo, E., Weller, R. A., and Straneo, F.: A data assimilative perspective of oceanic mesoscale eddy evolution during VOCALS-REx, Atmos. Chem. Phys., 13, 3329–3344, doi:10.5194/acp-13-3329-2013, 2013.
Thamdrup, B., Dalsgaard, T., and Revsbech, N. P.: Widespread functional anoxia in the oxygen minimum zone of the eastern South Pacific, Deep-Sea Res. Part I, 65, 36–45, 2012.
Winkler, L. W.: Bestimmung des im Wasser gelösten Sauerstoffs, Ber. Dtsch. Chem. Ges., 21, 2843–2855, 1888.

BGD
10, 9179–9211, 2013

Biogeochemistry anomalies in eddies off Peru

L. Stramma et al.

Table 1. Anomalies of mean anticyclonic (AE) and cyclonic (CE) eddies computed for the region 10° S to 20° S (Chaigneau et al., 2011) and for the 3 eddies A, B and C to a depth of 600 m although the vertical extent is even larger. Available heat anomaly (AHA) and available salt anomaly (ASA) within one eddy are computed following (Chaigneau et al., 2011).

	Chaigneau et al. (2011) (AE)	(CE)	A (AE)	B (AE)	C (CE)
Vertical extent (m)	0–450	0–200	0–600	0–600	0–600
Radius (km)	57.6	62.3	52.0	48.8	88.0
Volume ($\times 10^{12}$ m^3)	4.9	2.6	5.2	4.7	14.8
AHA ($\times 10^{18}$ J)	6.5	−5.9	17.7	3.7	−49.8
ASA ($\times 10^{10}$ kg)	17.4	−14.7	36.5	18.7	−98.8

BGD
10, 9179–9211, 2013
Biogeochemistry anomalies in eddies off Peru
L. Stramma et al.

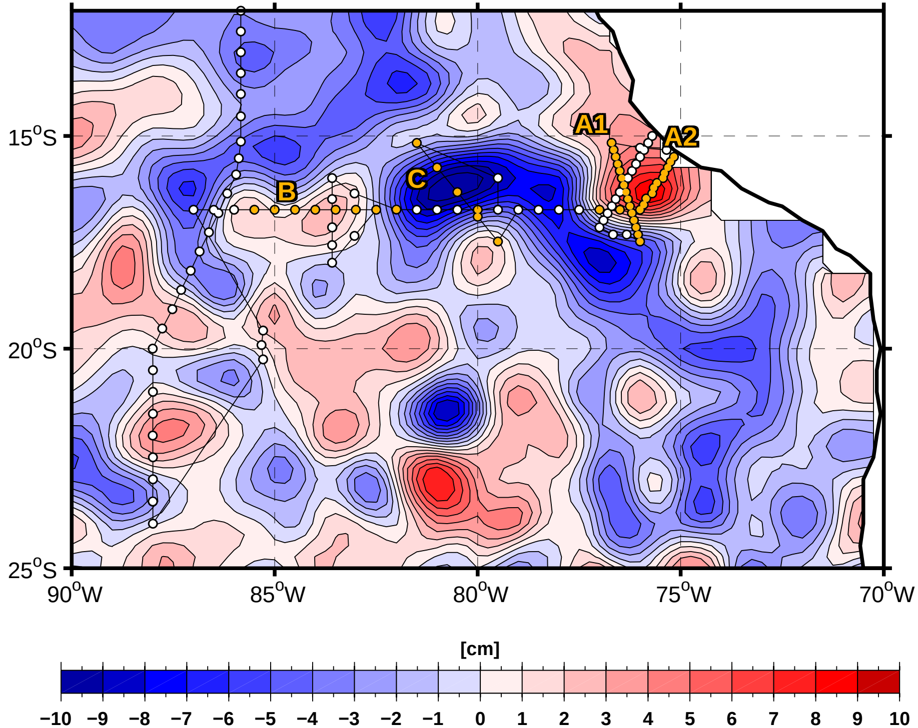

Fig. 1. Aviso sea level height anomaly (in cm) for 21 November 2012 and cruise track (black line) and CTD stations (white and yellow dots) of RV *Meteor* cruise M90. Stations used for sections plots are marked by yellow dots and are named A1, A2, B and C. Cyclonic features are shown in blue, anticyclonic ones in red.

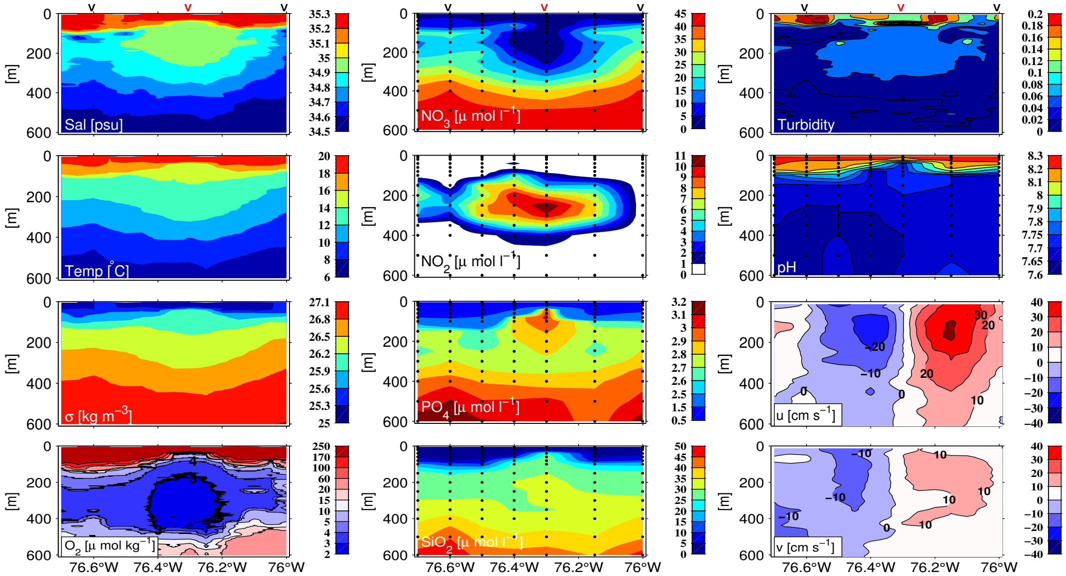

Fig. 2. Parameter distribution in the anticyclonic eddy A off the Peruvian shelf along a section A1 from 15° 10′ S, 76° 42′ W to 17° 30′ S, 76° W (see Fig. 1) for salinity, temperature, density and oxygen concentrations (left), nitrate, nitrite, phosphate and silicate concentrations (middle) and turbidity, pH and ADCP velocity components (right). For bottle data of the nutrient concentrations and pH the sampling depths are marked by black dots. To compute the eddy core anomalies in Fig. 3 the two outside profiles used are marked on top with a black v and the core profile with a red v.

BGD
10, 9179–9211, 2013

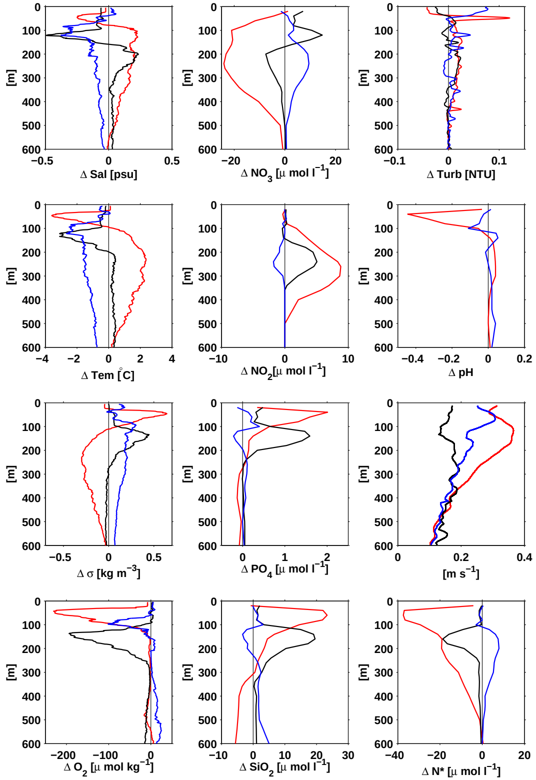

Fig. 3. Eddy core anomalies from the difference between profiles outside the eddy and in the eddy core (as shown in the section plots) versus depth for salinity, temperature, density and oxygen concentration (left), nitrate, nitrite, phosphate, and silicate concentration (middle), turbidity, pH, swirl velocity and N* (right) for the near-shelf anticyclonic eddy A (see Fig. 2) between 76.6° W and 76° W (red lines), the open ocean anticyclonic eddy B (see Fig. 7) between 85° 30′ W and 82° 30′ W (black lines) and the cyclonic eddy C (see Fig. 8) between 15° S and 17.5° S (blue lines).

BGD
10, 9179–9211, 2013
Biogeochemistry anomalies in eddies off Peru
L. Stramma et al.

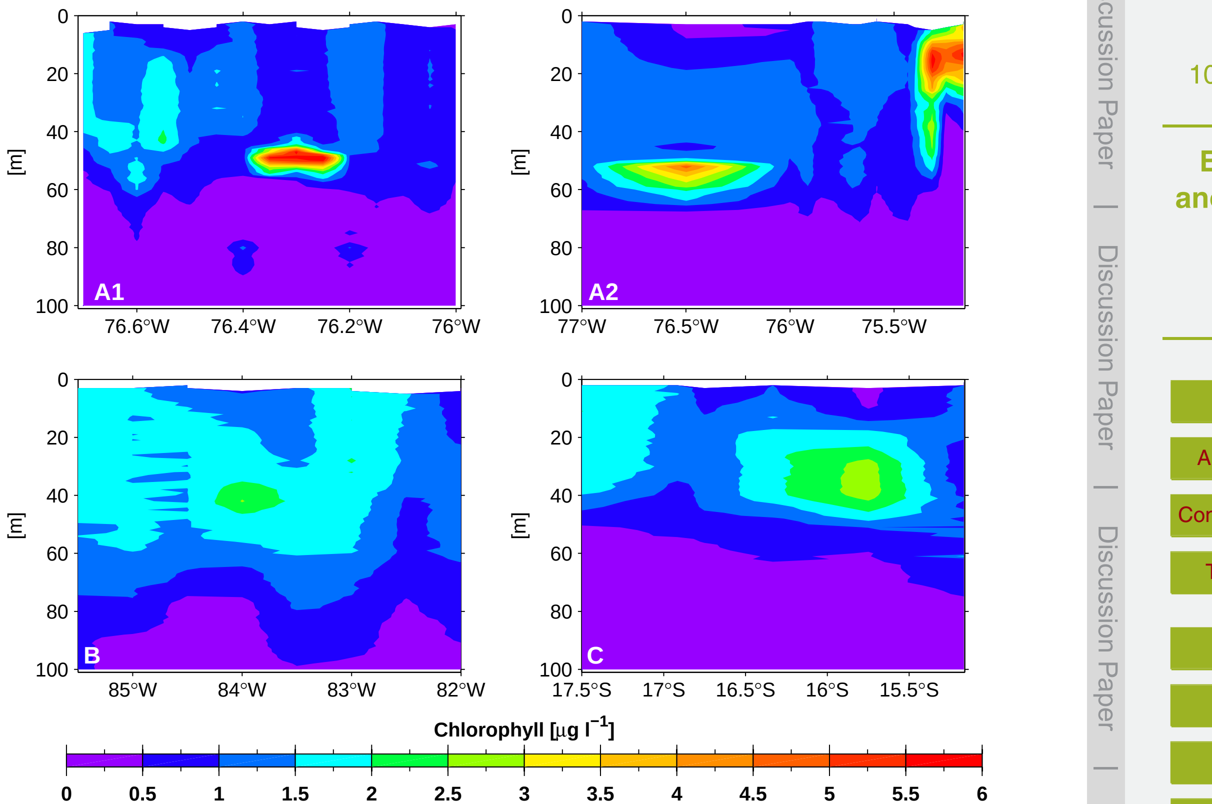

Fig. 4. Chlorophyll distribution in the upper 100 m for the anticyclones A, section A1 from 15° 10′ S, 76° 42′ W to 17° 30′ S, 76° W (top left; see Fig. 2), section A2 along 16° 45′ S to the shelf (top right; see Fig. 6), B along 16° 45′ S between 85° 30′ W and 82° W (bottom left; see Fig. 7) and the cyclone C between 17° 30′ S, 79° 30′ W and 15° 10′ S, 81° 30′ W (bottom right; see Fig. 8).

BGD
10, 9179–9211, 2013

Biogeochemistry anomalies in eddies off Peru

L. Stramma et al.

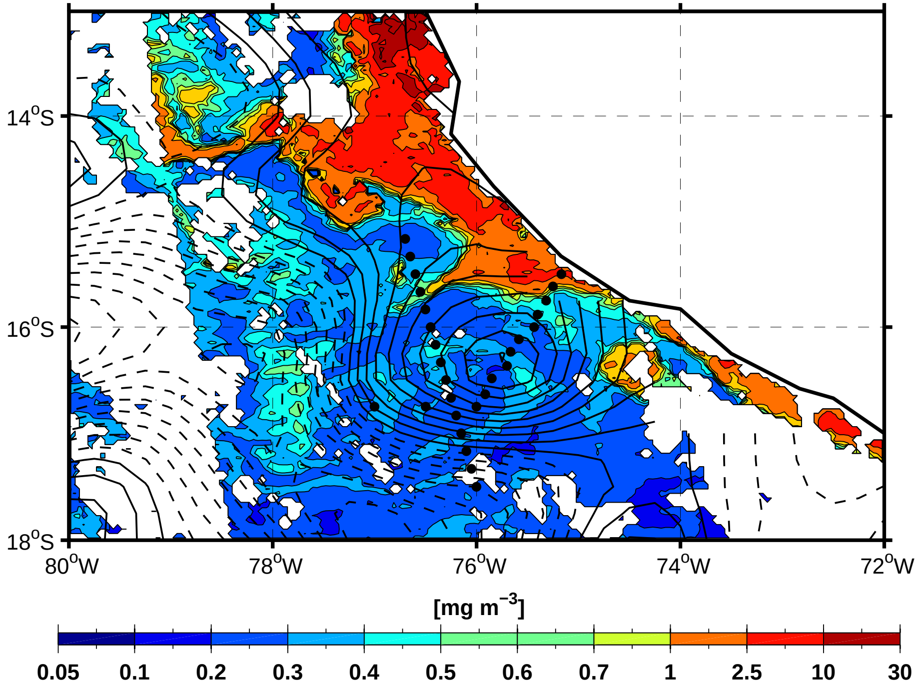

Fig. 5. Sea surface chlorophyll distribution (in mg m^{-3}) for 16 to 24 November 2012 from MODIS-aqua (color) with SSHA (in cm; contour interval 1 cm) for 21 November 2012 (black lines) as shown in Fig. 1.

BGD
10, 9179–9211, 2013

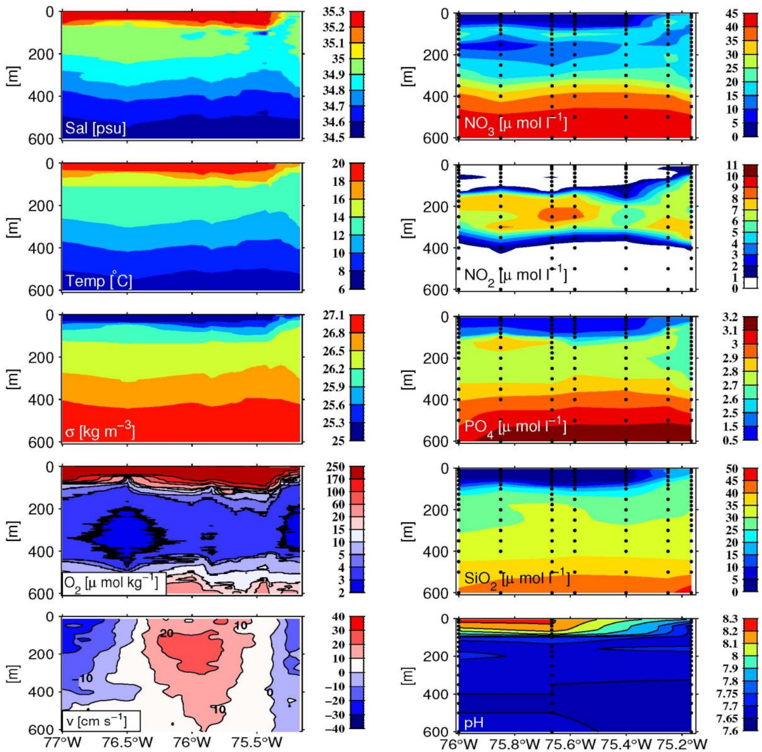

Fig. 6. Parameter distribution in the anticyclonic eddy A, section A2 off the Peruvian shelf from 77° W, 16° 45′ S to 76° W along 16° 45′ S and then northeastward to 75° 09′ W, 15° 30′ S (see Fig. 1) for salinity, temperature, density, oxygen concentrations and meridional velocity component (left) and the eastern part of section A2 only as no bottle data were collected between 76° W and 77° W from 76° W, 16° 45′ S to 75° 09′ W, 15° 30′ S for concentrations of nitrate, nitrite, phosphate, silicate, and pH (right). For bottle data of the nutrient concentrations and pH the sampling depths are marked by black dots.

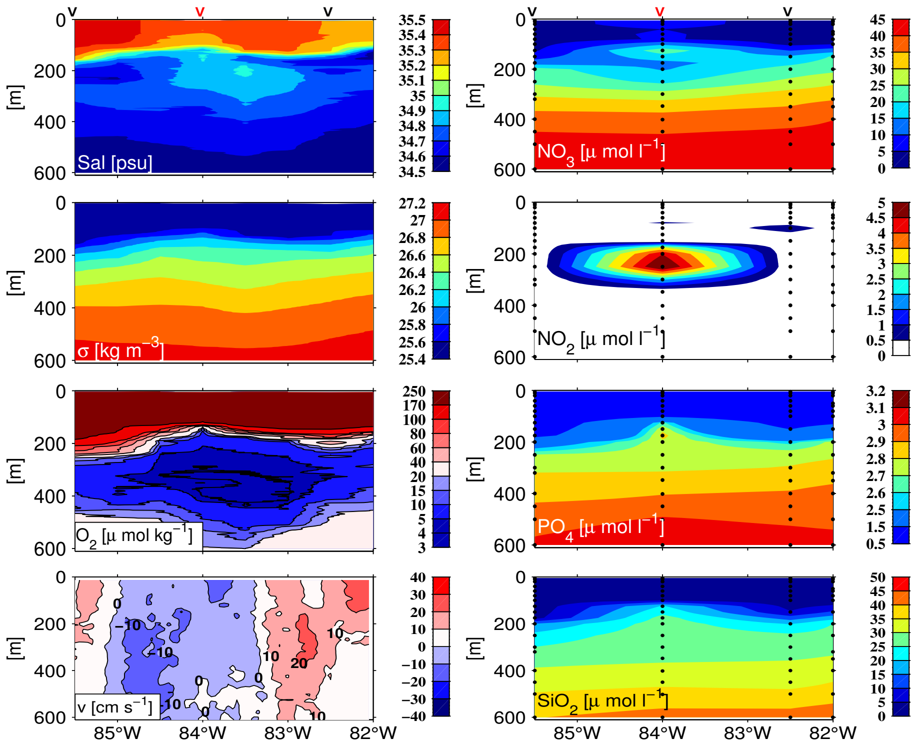

Fig. 7. Parameter distribution in the anticyclonic eddy B centered at about 83° 50′ W along 16° 45′ S between 85° 30′ W and 82° W for salinity, density, oxygen concentration and meridional velocity component (left) and nitrate, nitrite, phosphate and silicate concentration (right). For bottle data of the nutrient concentrations the sampling depths are marked by black dots. To compute the eddy core anomalies in Fig. 3 the two outside profiles used are marked on top with a black v and the core profile with a red v.

BGD
10, 9179–9211, 2013

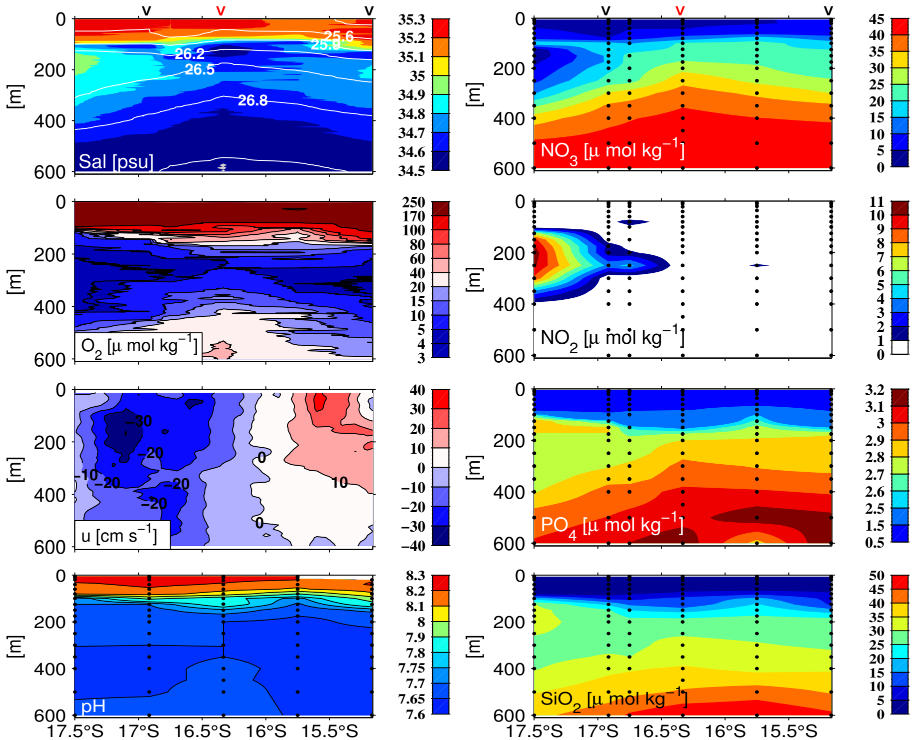

Fig. 8. Parameter distribution in the cyclonic eddy C on a diagonal section between 17° 30′ S, 79° 30′ W and 15° 10′ S, 81° 30′ W (see Fig. 1) for salinity, oxygen concentration, zonal velocity component and pH (left) and nitrate, nitrite, phosphate and silicate concentration (right). For bottle data of the nutrient concentrations and pH the sampling depths are marked by black dots. Selected isopycnals are included as white lines in the salinity section. To compute the eddy core anomalies in Fig. 3 the two outside profiles used are marked on top with a black v and the core profile with a red v.